Thermal Science and Engineering Progress 64 (2025) 103739

Contents lists available at ScienceDirect

Thermal Science and Engineering Progress

journal homepage: www.sciencedirect.com/journal/thermal-science-and-engineering-progress

Numerical analysis of heat transfer and tissue deformation in liver cancer during microwave ablation: A comparison of bioheat and porous media models

Wutipong Preechaphonkul [a], Vannakorn Mongkol [b], Arnon Sakonkanapong [c,*], Phadungsak Rattanadecho [b,**]

[a] Department of Prosthodontics, Faculty of Dentistry, Chulalongkorn University, 34 Henri Dunant Road, Wang Mai, Pathum Wan, Bangkok 10330, Thailand
[b] Hub of Talents Electromagnetic Energy Utilization in Medical Engineering, Department of Mechanical Engineering, Faculty of Engineering, Thammasat University, Khlong Luang, Pathum Thani, 12120, Thailand
[c] Mechatronics Department, KOSEN-KMITL, King Mongkut's Institute of Technology Ladkrabang, 1 Chalong Krung 1 Alley, Lat Krabang, Bangkok 10520, Thailand

ARTICLE INFO

Keywords:
Bioheat
Liver cancer
Microwave ablation
Numerical simulation
Porous media
Tissue deformation

ABSTRACT

This study presents a numerical comparison of microwave ablation using the Pennes bioheat and porous media models in a deformed liver cancer geometry. A single slot coaxial antenna operating at 2.45 GHz with a power of 10 W for 10 min was simulated using the finite element method, incorporating electromagnetic wave propagation, heat transfer, and tissue deformation. Validation against published experimental data and a mesh independence test confirmed the accuracy of the model. Results indicate up to a 6.7 % higher specific absorption rate in the porous media approach, contributing to a temperature difference of approximately 10–13 % at 10 min compared to the Pennes model. Peak von Mises stress increased by more than 2 Pa in tumor regions, and necrosis progression differed between the models. While both models predicted complete tumor cell death, the Pennes bioheat approach consistently reached thresholds sooner in both tumor and adjacent healthy tissue. These findings highlight the role of tissue porosity and convection in heat transport and deformation, demonstrating the porous media model's improved predictive capability for longer ablation durations and its potential for optimizing treatment protocols.

1. Introduction

Microwave ablation (MWA) is an alternative treatment for liver cancer, offering a minimally invasive option that can effectively target and destroy tumor cells while preserving the surrounding healthy tissue [1,2]. The use of MWA via a microwave coaxial antenna (MCA) in liver cancer treatment has shown promising results, making it an area of interest for further investigation. Liver cancer remains a complex disease with limited treatment options and high mortality rates [3]. MWA has emerged as a viable treatment, providing improved outcomes and reduced side effects compared to traditional therapies. However, the challenge of accurately targeting tumor cells without causing unintended damage to surrounding healthy tissue remains a limitation [4]. Hence, numerical simulation is essential for understanding MWA behavior in liver tissue and optimizing treatment parameters [5].

Following the recognition of MWA as an innovative treatment for liver cancer, the development of numerical models has become crucial for optimizing its effectiveness. These models are fundamental in simulating temperature distribution, a key factor in the success of MWA treatments [6]. Initially, MWA modeling was based on the Pennes bioheat equation, which incorporates heat diffusion and blood perfusion effects in tissues [7]. While this model provides foundational insights, it struggles to accurately capture the rapid heating phenomenon characteristic of MWA, prompting the exploration of enhanced models such as the Dual Phase Lag (DPL) bioheat model [8–11], modifications for water evaporation effects [12], and the incorporation of tissue deformation analysis to improve treatment accuracy [13].

* Corresponding author at: Mechatronics Department, KOSEN-KMITL, King Mongkut's Institute of Technology Ladkrabang, 1 Chalong Krung 1 Alley, Lat Krabang, Bangkok, 10520, Thailand.
** Corresponding author at: Hub of Talents Electromagnetic Energy Utilization in Medical Engineering, Department of Mechanical Engineering, Faculty of Engineering, Thammasat University, Khlong Luang, Pathum Thani, 12120, Thailand.
E-mail addresses: arnon.sa@kmitl.ac.th (A. Sakonkanapong), ratphadu@engr.tu.ac.th (P. Rattanadecho).

https://doi.org/10.1016/j.tsep.2025.103739
Received 2 October 2024; Received in revised form 25 February 2025; Accepted 30 May 2025
Available online 25 June 2025

Nomenclature

A	frequency factor (1/s)
a	volumetric heat transfer area (1/m)
C	arbitrary constant (−)
C_p	specific heat capacity (J/kg•K)
E	elastic modulus (Pa)
$\vec{E}$	electric field (V/m)
E_a	activation energy (J/mol)
F	external body force (N/mˆ3)
f	microwave frequency (Hz)
$\vec{H}$	magnetic field (A/m)
h_{tb}	tissue interfacial heat transfer coefficient (W/m^2•K)
k	wave propagation constant (m^{-1})
k_0	free space wave number.
k_{th}	thermal conductivity (W/m•K)
P_{in}	microwave Power input (W)
r	r-axis in the cylindrical coordinate system (m)
Q_{ext}	external heat source term (W/m^3)
Q_{met}	metabolism heat source term (W/m^3)
Q_{perf}	blood perfusion term (W/m^3)
R	universal gas constant (J/mol•K)
R_{inner}	inner radius of dielectric (m)
R_{outer}	outer radius of dielectric (m)
T	temperature (°C)
t	time (s)
u	displacement vector (m)
V	blood velocity (m/s)
Z	wave impedance (Ω)
z	z-axis in the cylindrical coordinate system (m)

Greek letter

α	thermal expansion coefficient (1/°C)
β	coefficient (−)
ε	strain (−)
ε^{th}	thermal strain (−)
ε_r	relative permittivity (−)
ε_0	permittivity of free space (F/m)
θ_d	fraction of necrotic tissue (−)
ρ	density of tissue (kg/m^3)
σ	stress (Pa)
σ_e	electric conductivity (S/m)
λ	wavelength (m)
μ_r	relative permeability (−)
ν	poisson's ratio (−)
φ	azimuth-axis in the cylindrical coordinate system (m)
ϕ	porosity (−)
Ω	cumulative tissue damage (−)
ω	angular frequency (rad/s)
ω_b	blood perfusion rate of tissue (1/s)

Subscripts

b	blood phase
eff	effective value
r, z, φ	component of the cylindrical coordinate system
ref	reference
s	tissue phase
th	thermal properties

A promising alternative is the porous media approach, which leverages the microstructural similarity between tissues and porous materials to improve heat transfer modeling in biological tissues [14,15]. This theory has the potential to revolutionize MWA numerical modeling by providing a more nuanced understanding of thermal dynamics and blood flow heterogeneity [1,16,17]. Notably, recent studies by Tucci et al. [6] and Trujillo et al. [18] have applied variable-porosity models to MWA, demonstrating their significant impact on ablation outcomes. By considering tissue porosity and permeability, this approach aims to improve the accuracy of thermal predictions, potentially optimizing treatment strategies.

Despite the promise of porous media theory, its application in MWA treatment remains limited. Most existing models focus on homogeneous tissue assumptions, neglecting the dynamic variations in tissue porosity, blood perfusion, and mechanical response during ablation. The complexity of simulating heat transfer in MWA using porous media theory, which involves multiple assumptions and parameters, highlights a significant research gap. Addressing these gaps through focused studies on heat transport under porous media conditions in MWA treatment is essential for enhancing model accuracy, treatment precision, and overall patient safety.

In previous numerical models for MWA treatment, tissue deformation due to thermal expansion has been identified as a critical factor affecting heat transport. As microwave energy propagates and converts into localized heat, a rapid increase in tissue temperature leads to thermal expansion, which influences heat transport dynamics [19,20]. Keangin et al. [13] compared MWA models with and without tissue deformation analysis, demonstrating its substantial impact on heat distribution. These findings indicate that tissue deformation is not merely a by-product of the heating process but a fundamental factor influencing treatment planning, efficacy, and patient safety.

Despite its importance, few studies have integrated porous media theory with tissue deformation analysis in MWA treatment. This presents a significant research gap, as the mechanical response of tissues can affect both heat transfer and electromagnetic wave propagation. Investigating these effects in detail will help refine MWA numerical models, enhancing treatment precision and safety.

This study presents a numerical analysis of liver cancer models under the Pennes bioheat and porous media approaches, comparing and investigating electromagnetic wave propagation, temperature distribution, and tissue deformation. The mathematical model integrates electromagnetic propagation, heat transfer in biological tissues, tissue damage assessment, and tissue deformation analysis. A key aspect of this research is the direct comparison of tissue deformation effects between the Pennes bioheat and porous media models under identical conditions. To ensure the accuracy of the numerical simulations, results are validated against experimental data from Yang et al. [12]. The Finite Element Method (FEM) is employed to solve the governing equations. Simulation results provide insights into heat transport mechanisms and tissue deformation dynamics during MWA treatment, emphasizing the key differences between Pennes bioheat and porous media models. These findings offer valuable guidance for treatment planning and contribute to improving model accuracy in MWA simulations.

2. Problem statement

This study focused on comparing the phenomena observed in deformed liver cancer treatment using MWA, between models developed based on the Pennes bioheat approach and those utilizing the porous media approach. In this investigation, the deformed liver cancer models were treated using a single-slot microwave coaxial antenna, a device widely recognized and used in practical applications [1]. To simplify the complexity of this issue, it is assumed that the microwave antenna is already embedded in the liver tissue and remains stationary

during the treatment procedure. In this study, the microwave antenna operates at a power level of 10 W and a frequency of 2.45 GHz for all cases. The geometric dimensions and properties of the single-slot MCA will be discussed in the following section. The model comprises three domains: the single slot MCA, the tumor, and the surrounding healthy liver tissue. Mathematical models were developed based on electromagnetic wave propagation, heat transfer in biological tissues, tissue damage, and tissue deformation analysis. Electromagnetic wave propagation is considered across all domains. On the other hand, heat transfer in biological tissues, tissue damage analysis, and tissue deformation analysis are confined to the biological domain, specifically the tumor and surrounding healthy tissue. The mathematical models were solved using FEM, based on the assumption of 2D transient axisymmetric. The specific absorption rate (SAR), temperature distribution, tissue deformation, and the fraction of necrotic tissue are calculated and compared between models developed using the Pennes bioheat approach and the porous media approach. Particular emphasis was placed on the effects of tissue deformation analysis, highlighting the distinctions and implications of using the porous media and bioheat approaches to model the dynamic responses of tissue to MWA. A critical aspect of this study involves examining the phenomena during the treatment process, explicitly comparing models developed using the Pennes bioheat approach with those utilizing the porous media approach, focusing on tissue deformation. This examination is instrumental in understanding the nuanced impacts of different modeling approaches on the efficacy of MWA treatments.

3. Materials and methods

The numerical model is formulated to predict SAR distribution, temperature profile, tissue damage, and tissue deformation in a liver cancer model during MWA treatment. The following section presents an analysis of electromagnetic wave propagation, heat transfer, tissue damage, and tissue deformation in liver cancer during the MWA process. The system of governing equations, along with the initial and boundary conditions, is solved numerically using FEM implemented in COMSOL™ Multiphysics. The relevant boundary conditions are depicted in Fig. 1.

3.1. Physical model

This study develops a physical model using a 2D axisymmetric approach in r-z coordinates to simulate MWA treatment. The model's overall dimensions include a radial axis of 30 mm and a height of 80 mm, consistent with the typical dimensions of human organs [4,5,12]. The practical concept of this treatment is illustrated in Fig. 1(a). In clinical applications, MWA is inherently a three-dimensional (3D) problem, as shown in Fig. 1(b). To simplify computational complexity, the liver is assumed to be homogeneous, and the treatment domain is considered axisymmetric, reducing the 3D problem to a 2D axisymmetric model, as depicted in Fig. 1(c). The model comprises three key domains: the microwave antenna, the tumor, and the surrounding healthy liver tissue.

In practical applications, the microwave antenna used is a single-slot MCA, whose dimensions are well-documented in the literature [2,13]. The dielectric properties of the antenna are assumed to be constant and are provided in Table 1. In this study, heat transfer and deformation analysis of the antenna are not considered. The antenna is positioned along the z-axis and remains stationary during treatment, with its

Table 1
The dielectric properties of a single-slot microwave coaxial antenna (Keangin & Rattanadecho, 2013).

Properties	Relative permittivity, ε_r	Electric conductivity, σ_e (S/m)	Relative permeability μ_r
Dielectric	2.03	0	1
Catheter	2.1	0	1
Slot	1	0	1

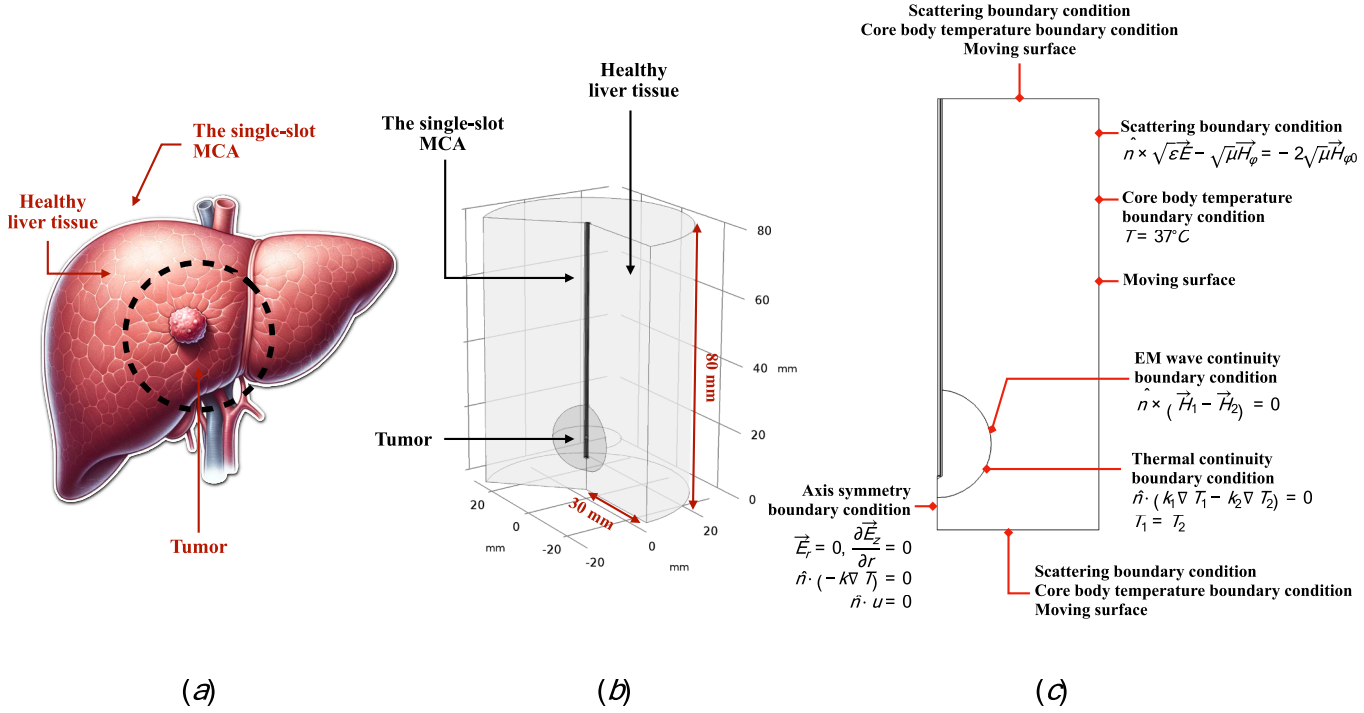

Fig. 1. Physical domain and boundary conditions of MWA for liver cancer treatment model; (a) The concept of MWA for deformed liver cancer treatment, (b) The model geometry showing the arrangement of the liver, tumor, and MCA, (c) The boundary conditions applied to the models.

insertion point at the top boundary of the cylindrical domain, as shown in Fig. 1(b).

The tumor is modeled as a spherical structure with a radius of 10 mm. Although real tumors exhibit asymmetry, they are conventionally approximated as spherical to facilitate modeling and ensure comprehensive ablation of cancer cells [4,5]. In this study, the tumor center is positioned along the z-axis, 16 mm away from the bottom boundary, aligning with the slot centerline of the antenna. Due to the 2D axisymmetric assumption, the tumor is represented as a semicircle, as illustrated in Fig. 1(c).

The healthy liver tissue domain surrounds both the antenna and the tumor. In this study, healthy liver tissue is assumed to be homogeneous and isotropic, similar to the tumor. The thermal, dielectric, and mechanical properties of both tissue types are summarized in Table 2 [6,18,21,22], with all properties evaluated at 2.45 GHz, the operating frequency of MWA.

The physical domain is thus represented as a 2D rectangular geometry along the r and z axes under the 2D axisymmetric framework. This formulation serves as the foundation for deriving the governing equations, boundary conditions, and initial conditions in cylindrical coordinates. Consequently, the model effectively bridges 1D, 2D, and 3D representations, ensuring a realistic and computationally efficient simulation of MWA treatment.

3.2. Electromagnetic wave propagation analysis

Electromagnetic wave propagation analysis plays a critical role in MWA treatment. The treatment mechanism involves microwave energy transmission through MCA, which is subsequently absorbed by the tumor and surrounding healthy tissue, generating localized heat within a specific region. Since electromagnetic wave propagation directly influences temperature distribution, it is a key factor in determining the effectiveness of the treatment. Therefore, this mathematical model is developed with a primary focus on electromagnetic wave propagation analysis across all domains.

To simplify the complexity of the analysis, the following assumptions are considered:

1. Electromagnetic wave propagation is analyzed within a 2D axisymmetric model in r-z coordinates.
2. In the MCA, electromagnetic wave propagation is characterized by transverse electromagnetic (TEM) fields.
3. In the healthy tissue and tumor, electromagnetic wave propagation is characterized by transverse magnetic (TM) fields.
4. The dielectric properties of the MCA are assumed to be constant and uniform.

The propagation of electromagnetic waves within the microwave antenna follows the TEM model as described in previous studies [13].

Table 2
The properties of the healthy liver tissue, the tumor, and blood (Lopresto et al. 2017; Trujillo et al., 2020; Tucci et al, 2022).

Properties	The healthy liver tissue	Tumor	Blood
Relative permittivity, ε_r	57.55	62.44	–
Electric conductivity, σ_e (S/m)	1.95	2.18	–
Density, ρ (kg/m^3)	1,080[a] / 370[b]	1045[a] / 370[b]	1000[a] / 370[b]
Thermal conductivity, k_{th} (W/m•K)	0.502	0.60	0.502
Specific heat capacity, C_p (J/kg•K)	3,455[a] / 2,156[b]	3,760[a] / 2,156[b]	3,639[a] / 2,156[b]
Blood perfusion, ω_b (1/s)	0.0036	0.019	–
Elastic modulus, E (kPa)	0.6	20	–

[a] Temperature below 100 °C [b] Temperature above 100 °C.

Electric field ($\vec{E}$):

$$\vec{E} = \vec{u}_r \frac{C}{r} exp(j(\omega t - kz)), \tag{1}$$

Magnetic field ($\vec{H}$)

$$\vec{H} = \vec{u}_\varphi \frac{C}{rZ} exp(j(\omega t - kz)), \tag{2}$$

where $C = \frac{ZP_{in}}{\pi \ln(R_{outer}/R_{inner})}$ is the arbitrary constant, Z is the wave impedance in the dielectric of the cable (Ω), P_{in} is the microwave power input (W), R_{outer} is the dielectric outer radius (m), R_{inner} is the dielectric inner radius (m), f is the microwave frequency (Hz), $\omega = 2\pi f$ is the angular frequency (rad/s), k is the wave propagation constant (m^{-1}), which relates to the wavelength (λ) in medium: $k = \frac{2\pi}{\lambda}$.

Furthermore, the propagation of the electromagnetic wave in the healthy liver tissue and the tumor is by TM as described by the following equation:

$$\nabla \times \left(\left(\frac{1}{\varepsilon_r} - \frac{j\sigma_e}{\omega \varepsilon_0} \right)^{-1} \nabla \times \vec{H}_\varphi \right) - \mu_r k_0^2 \vec{H}_\varphi = 0 , \tag{3}$$

where the $\vec{H}_\varphi$ is magnetic field intensity (A/m), μ_r is relative permeability, ε_r is relative permittivity, $\varepsilon_0 = 8.8542 \times 10^{-12}$ (F/m) is permittivity of free space, σ_e is the electrical conductivity (S/m), and k_0 is the free space wave number.

In this study, the relative permittivity (ε_r) and the electric conductivity (σ_e) of the healthy liver tissue and tumor are considered to be temperature-dependent, as detailed in [22]. The function is as follows:

$$\sigma_e(T) = \sigma_e(T = 37\,^\circ\mathrm{C}) \left(1 - \frac{1}{1 + exp(6.583 - 0.0598T)} \right), \tag{4}$$

$$\varepsilon_r(T) = \varepsilon_r(T = 37\,^\circ\mathrm{C}) \left(1 - \frac{1}{1 + exp(5.223 - 0.0524T)} \right), \tag{5}$$

where the $\sigma_e(T)$ is the electrical conductivity at temperature T °C, $\varepsilon_r(T)$ is the relative permittivity at temperature T °C, and T is the tissue temperature. The dielectric properties of MCA, the tumor, and liver tissue are shown in the Table 1 and 2.

The interaction of electromagnetic waves within the domain of the healthy tissue and the tumor is characterized by the distribution of SAR. As electromagnetic waves are emitted by MCA, they traverse this antenna and subsequently propagate through the entirety of the domain. These waves are absorbed, leading to their conversion into an external heat source term (Q_{ext}). In the context of this study, the SAR is defined as the rate of microwave power absorption per unit mass of tissue (W/kg) [17]. The formulation of SAR is as follows:

$$SAR = \frac{\sigma_e}{2\rho} \left| \vec{E} \right| = \frac{Q_{ext}}{\rho}, \tag{6}$$

where ρ is the density of the healthy liver tissue (kg/m^3) and the tumor (kg/m^3).

The boundary conditions of electromagnetic wave propagation show in Fig. 1(c), and the electric and magnetic field at the initial condition is set to zero.

3.3. Heat transfer analysis

This treatment is designed to induce thermal damage within a specific region, such as a tumor, while minimizing damage to surrounding healthy tissue. Heat transfer analysis plays a pivotal role in evaluating the treatment's efficacy. This study examines deformed liver cancer models developed under two distinct heat transfer methodologies: the Pennes bioheat approach and the porous media approach. The analysis

focuses on heat transfer dynamics within both healthy liver tissue and tumor regions during MWA treatment.

The bioheat equation serves as the foundation for modeling heat transfer within biological tissue. However, the primary focus of this study lies in comparing the Pennes bioheat model and the porous media model, emphasizing key differences in their bioheat equations. To simplify the complexity of the analysis, the following assumptions are considered:

1. Heat transfer analysis is conducted within a 2D axisymmetric model in r-z coordinates.
2. For the Pennes bioheat approach, both the healthy liver tissue domain and the tumor domain are assumed to be homogeneous with uniform properties.
3. For the porous media approach, both the healthy liver tissue and tumor domains are considered porous, isotropic, and fully saturated with blood.
4. In the porous media approach, the local temperature between the tissue and blood phases at the same point is assumed to be in local thermal equilibrium (LTE).
5. The porosity of the healthy liver tissue and tumor is considered constant throughout the treatment process.
6. Blood within the tissue is assumed to be incompressible and follows Newtonian fluid dynamics.
7. Chemical reactions and phase changes within the tissue are neglected.
8. Heat transfer analysis within the MCA domain is neglected.

The Pennes bioheat equation models heat transfer in biological tissue by solving the energy equation under the bioheat approach [7]. The equation is as follows:

$$\rho C_p \frac{\partial T}{\partial t} = \nabla \bullet (k_{th} \nabla T) + Q_{perf} + Q_{met} + Q_{ext} \ , \tag{7}$$

where the ρ is the density of the healthy tissue (kg/m^3), the tumor (kg/m^3), and blood (kg/m^3), C_p is the specific heat capacity (J/kg•K), T is temperature of the healthy tissue and the tumor (°C), k_{th} is the thermal conductivity (W/m•K), Q_{perf} is the blood perfusion term (W/m^3), Q_{met} is the metabolism heat source term (W/m^3), and Q_{ext} is the external heat source term (W/m^3).

The thermal properties of both healthy tissue and tumor are presented in Table 2. Additionally, perfusion physically represents a heat sink, as it accounts for heat transfer from heated tissue to circulating blood, which occurs due to the temperature difference between the tissue and blood [6,16]. The heat sink effect due to perfusion, denoted as Q_{perf}, is defined as:

$$Q_{perf} = \beta \rho_b C_{p,b} \omega_b (T_b - T), \tag{8}$$

where ω_b is the blood perfusion rate in the healthy liver tissue (1/s), and the tumor (1/s), which is characterized by the blood perfusion rate, which can be intended as the frequency at which blood perfuses the tissue. The coefficient β is related to the thermal damaged function, and it will be described in the following subsection.

The governing equations that describe heat transfer in biological porous tissue for tissue and blood phases have been modified to incorporate LTE conditions [1,5]. The equation is as follows:

$$\left(\rho C_p\right)_{eff} \frac{\partial T}{\partial t} + \phi \left(\rho C_p\right)_b (V \bullet \nabla T) = \nabla \bullet \left(k_{th,eff} \nabla T\right) + (1-\phi) Q_{met} + Q_{ext}, \tag{9}$$

$$\left(\rho C_p\right)_{eff} = (1-\phi)\left(\rho C_p\right)_s + \phi \left(\rho C_p\right)_b \ , \tag{10}$$

$$k_{th,eff} = (1-\phi) k_{th,s} + \phi k_{th,b}, \tag{11}$$

where *s, b, th* and eff represent tissue phase (solid matrix), thermal, blood phase, and the effective value respectively. The porosity (ϕ) is defined as the volume of the vascular space compared to the total volume, and in this study, it is assumed to be a constant value of 0.05 [1,16,23]. However, the blood velocity (V) is related to the volumetric heat transfer area (a) between blood and tissue phases, the tissue interfacial heat transfer coefficient (h_{tb}).

The boundary conditions of heat transfer of the healthy liver tissue and the tumor in the heat transfer analysis are shown in Fig. 1(c), and the temperature in the healthy tissue and the tumor at the initial condition is set to 37 °C as same as the core body temperature.

3.4. Thermal damaged analysis

The study of thermally damaged tissue is an integral aspect of heat transfer analysis, but it is considered only for healthy liver tissue and the tumor. The assumptions in this section are consistent with those established in the heat transfer analysis. Thermal damage refers to injury resulting from excessive heat exposure and can be quantified using the Arrhenius damage equation. This equation establishes a correlation between exposure time, temperature, and kinetic parameters, describing tissue morphology changes due to protein degradation during thermal ablation [2,3]:

$$\Omega(t) = A \int_0^t exp\left(\frac{-E_a}{RT}\right) dt, \tag{12}$$

where Ω(t) is the cumulative tissue damage, A is the frequency factor (1/s), E_a is the activation energy (J/mol) and R is the universal gas constant (J/mol•K). For the healthy liver tissue domain, the frequency factor (A), and activation energy (E_a) are equal to $A = 7.39 \times 10^{39}$ (1/s) and $E_a = 2.577 \times 10^5$ (J/mol). For the tumor domain, the frequency factor (A), and activation energy (E_a) are equal to $A = 3.247 \times 10^{43}$ (1/s) and $E_a = 2.814 \times 10^5$ (J/mol) [3]. The fraction of necrotic tissue (θ_d) can be expressed as:

$$\theta_d = 1 - exp(-\Omega), \tag{13}$$

The fraction of necrotic tissue (θ_d) is quantified as a proportion of the damaged tissue, with values ranging from 0 to 1. A value of one indicates complete tissue damage, whereas a value of zero signifies no damage. Furthermore, the coefficient β mentioned in the previous section is related to the fraction of necrotic tissue [6]. If the fraction of necrotic tissue is equal to or exceeds 0.99, the coefficient β is set to zero. Conversely, if the fraction of necrotic tissue is less than 0.99, the coefficient β is set to one.

3.5. Tissue deformation analysis

Tissue deformation analysis is essential for liver cancer treatment, as MWA involves the rapid heating of biological tissue, leading to thermal expansion. This analysis significantly influences temperature prediction, which is crucial for achieving effective treatment outcomes. To simplify the complexity of the analysis, the following assumptions are considered:

1. Tissue deformation analysis is conducted within a 2D axisymmetric model in r-z coordinates.
2. Both the healthy liver tissue and the tumor domain are considered to undergo elastic deformation.
3. The healthy liver tissue and the tumor are assumed to exhibit isotropic deformation characteristics.
4. The mechanical properties of the tissue are assumed to be uniform and constant throughout the MWA treatment.
5. Chemical reactions occurring during tissue deformation are disregarded.
6. Deformation analysis within the microwave antenna is not considered.

The analysis of tissue deformation within both healthy liver tissue and the tumor is intricately linked to the thermal effects experienced during MWA treatment. This analysis is conducted by solving the equilibrium equations, strain–displacement relations, and stress–strain relations [13]. The governing equations for this analysis are presented as follows:

Equilibrium equations

$$\frac{\partial \sigma_{rr}}{\partial r}+\frac{\partial \sigma_{rz}}{\partial z}+\frac{\sigma_{rr}-\sigma_{\varphi\varphi}}{r}+F_r=0, \tag{14}$$

$$\frac{\partial \sigma_{rz}}{\partial r}+\frac{\partial \sigma_{zz}}{\partial z}+\frac{\sigma_{rz}}{r}+F_z=0, \tag{15}$$

The strain–displacement relations

$$\varepsilon_{rr}=\frac{\partial u_r}{\partial r}, \tag{16}$$

$$\varepsilon_{zz}=\frac{\partial u_z}{\partial z}, \tag{17}$$

$$\varepsilon_{\varphi\varphi}=\frac{u_r}{r}, \tag{18}$$

$$\varepsilon_{rz}=\frac{1}{2}\left(\frac{\partial u_r}{\partial z}+\frac{\partial u_z}{\partial r}\right), \tag{19}$$

The stress–strain relations

$$\varepsilon_{rr}=\frac{1}{E}[\sigma_{rr}-\upsilon(\sigma_{\varphi\varphi}+\sigma_{zz})]+\varepsilon^{th}, \tag{20}$$

$$\varepsilon_{\varphi\varphi}=\frac{1}{E}[\sigma_{\varphi\varphi}-\upsilon(\sigma_{rr}+\sigma_{zz})]+\varepsilon^{th}, \tag{21}$$

$$\varepsilon_{rz}=\frac{\sigma_{rz}(1+\upsilon)}{E}, \tag{22}$$

where σ is the stress (Pa), u is the displacement vector (m), F is the external body force (N/m^3), ε is the strain ν is the poisson's ratio, E is the elastic modulus (Pa), and the thermal strain (ε^{th}) can be defined by the following as:

$$\varepsilon^{th}=\int_{T_{ref}}^{T}\alpha dT, \tag{23}$$

where, T_{ref} is the core body temperature ($T_{ref}=37$ °C), and the coefficient of thermal expansion, denoted as α (1/°C), for both healthy tissue and tumors is 1×10^{-4} 1/°C [13]. The mechanical properties of the healthy liver tissue and the tumor are shown in Table 2 [13,24,25].

The boundary condition of tissue deformation analysis of the healthy tissue and the tumor are shown in Fig. 1(c), and the stress and strain in the healthy tissue and the tumor at the initial are assumed to zero.

3.6. Calculation procedure

In this study, numerical models were analyzed using FEM to solve the 2D axisymmetric transient problem, utilizing COMSOL™ Multiphysics. The mathematical model for deformed liver cancer treatment with MWA integrates multiple analyses, including electromagnetic wave propagation, heat transfer in biological tissues, tissue damage, and tissue deformation. The model was discretized using triangular elements with Lagrange quadratic shape functions, incorporating adaptive refinement in sensitive regions to enhance accuracy.

The computational scheme begins by computing the external heat source term, which is determined by first running an electromagnetic wave propagation calculation to obtain SAR. Subsequently, the time-dependent temperature distribution is solved. Additionally, thermal damage and tissue deformation due to thermal expansion are computed. Both the Pennes bioheat model and the porous media model follow the same computational procedure.

To accurately describe the heat transfer pattern, the specification of temperature distribution is required. These equations are coupled with the governing equations for electromagnetic wave propagation, energy conservation, the Arrhenius equation, and tissue deformation. The initial and maximum time steps used to solve the system of equations for electromagnetic wave propagation and heat transport are 1×10^{-12} s and 0.1 s, respectively.

The 2D axisymmetric FEM model is discretized using triangular elements with Lagrange quadratic shape functions, as illustrated in Fig. 2 (a). To ensure accurate results, a fine mesh is applied in sensitive areas where significant thermal and mechanical changes occur. The system of partial differential equations, along with their corresponding boundary conditions, is coupled and solved numerically using FEM in COMSOL™ Multiphysics. FEM provides efficient and accurate solutions to complex heat transfer problems, making it well suited for simulating thermal ablation processes.

The Multifrontal Massively Parallel Solver (MUMPS) is employed as a direct solver, while the Generalized Minimal Residual Method (GMRES) is used as an iterative solver to approximate the SAR profile, temperature distribution, and tissue deformation caused by thermal expansion.

To ensure solution accuracy and mesh independence, the study examines model convergence by analyzing temperature variations at a critical point. The mesh density, with 47,095 elements, was verified to achieve mesh-independent results, as shown in Fig. 2(b). The convergence curve demonstrates the relationship between temperature and the number of elements, confirming that beyond a certain element count, additional refinement does not significantly impact computational outcomes. A dense mesh zone is applied around the antenna tip, where temperature gradients are highest, ensuring accurate representation of thermal effects.

4. Results and discussion

A comprehensive numerical model is proposed, integrating transient heat transfer and tissue deformation, coupled with the electromagnetic wave propagation equation, to describe the SAR profile, temperature distribution, tissue damage, and tissue deformation. In the following section, a systematic investigation is conducted to compare the bioheat and porous media approaches in terms of SAR distribution, temperature profile, and tissue deformation in a liver cancer model during the MWA process.

4.1. Model verification

This study conducted a validation of the numerical model to ensure the accuracy of simulation outcomes for deformed liver cancer treatment using MWA. The validation process involved comparing the numerical model's results with experimental data reported by Yang et al. [12] under identical experimental conditions. For this purpose, the microwave power input was set at 75 W with an operating frequency of 2.45 GHz. The initial temperature within the liver domain was set at 8 °C, with the MCA inserted to a depth of 20 mm into bovine liver tissue, and the heating period was fixed at 50 s.

Fig. 3 presents a comparison between the simulation results and the experimental data from Yang et al. [12], specifically illustrating temperature variations at two locations positioned 4.5 mm and 9.5 mm from the antenna over the heating duration. The simulation results showed strong agreement with the experimental findings, as reflected in the R squared values provided in Table 3. This comparison underscores the precision and reliability of the numerical model.

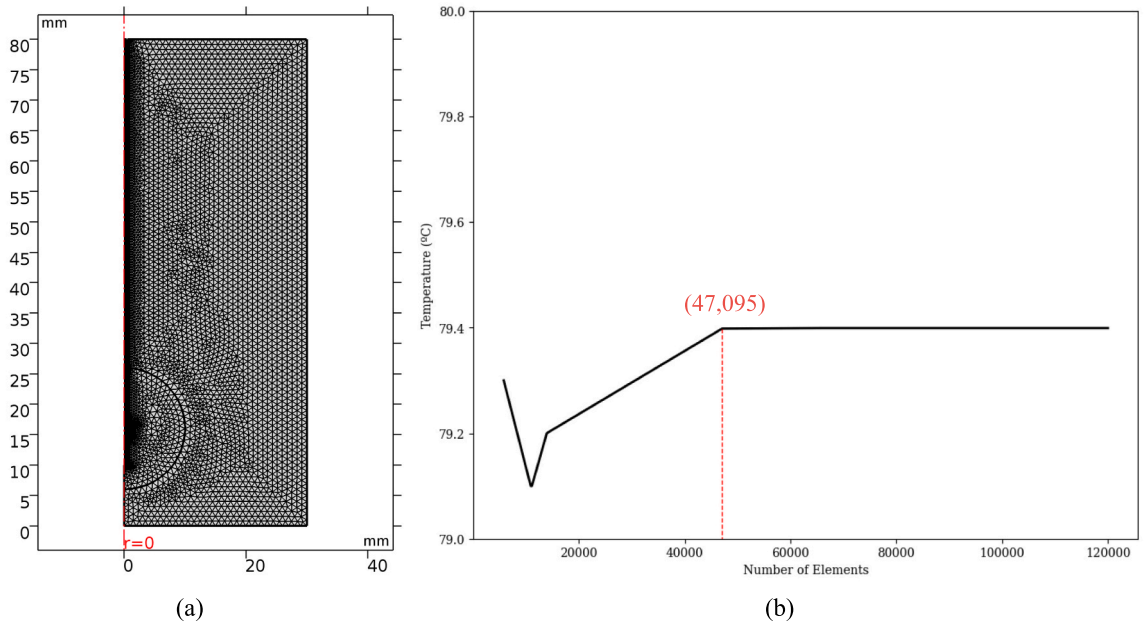

Fig. 2. Mesh configuration and convergence analysis; (a) FEM mesh used for the deformed liver tissue during MWA treatment model, (b) Mesh convergence of deform porous model.

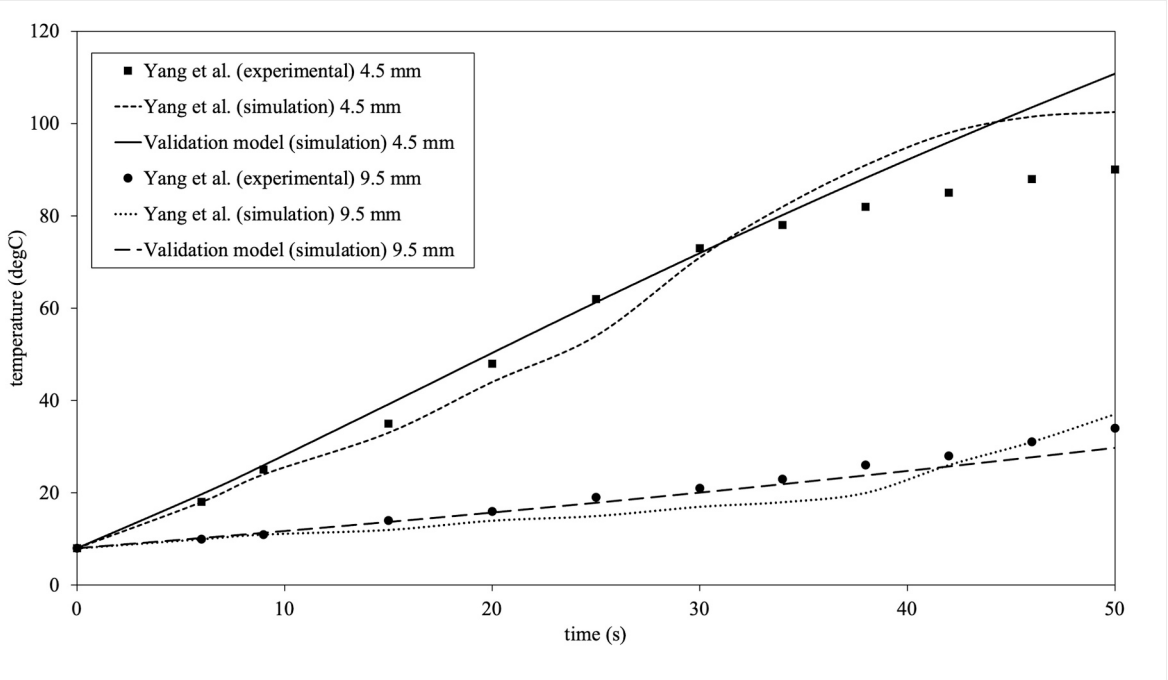

Fig. 3. Validation of the tissue temperature by current study compare with experimental result obtained by Yang et al. [9].

Table 3
Comparisons of R-Squared of the liver tissue temperature between the presented model and Yang et al. (Yang et al., 2007).

Position	Comparisons of R-Squared with experiment from Yang et al.	
	Presented study	Yang et al. (simulation model)
4.5 mm	0.91	0.92
9.0 mm	0.94	0.86

4.2. Electromagnetic wave propagation analysis

Electromagnetic wave propagation plays a crucial role in MWA treatments, as the fundamental principle of MWA involves targeting the tumor with microwave energy delivered through an antenna. The nature of wave propagation, influenced by multiple factors, significantly affects the generation of localized heat during the procedure. To enable a comprehensive investigation and comparison of deformed liver cancer models treated with MWA using either the Pennes bioheat approach or

the porous media approach, a detailed analysis of electromagnetic wave propagation is essential. In this study, electromagnetic wave propagation is characterized in terms of SAR distribution, which quantifies the electromagnetic energy absorbed within a localized region.

Fig. 4(a) presents the 3D SAR profile in a deformed liver cancer model subjected to the porous media approach during MWA, after a treatment duration of 10 min. This figure highlights the volumetric heating effect, a defining characteristic of the MWA process. The microwave energy, emitted from the antenna, propagates through both the tumor and healthy liver tissue, inducing localized heat generation through dielectric heating. The SAR intensity is highest around the slot area and decreases with increasing distance from the slot. The SAR profile pattern exhibits a water droplet-like shape, with higher SAR values observed within the tumor compared to healthy liver tissue. A comparison of 3D SAR profiles between the Pennes bioheat approach and the porous media approach reveals similar overall patterns; therefore, only a representative Fig. 4(a) is provided for illustration.

Additionally, Fig. 4(a) highlights the insertion depth line, which runs parallel to the MCA and is positioned 2.5 mm from the antenna centerline. Fig. 4(b) presents the SAR distribution along the insertion depth line after a treatment duration of 10 min. This figure demonstrates that the SAR distribution patterns under both the Pennes bioheat approach, and the porous media approach exhibit similar trends with SAR values peaking around the slot area and decreasing with distance. The mean absolute difference between the two models is calculated as 0.0785 kW per kg, corresponding to approximately 6.72 % in overall deviation. However, while the overall SAR distribution patterns are comparable, differences in SAR magnitude particularly in the peak SAR region are evident between the two models.

The heat transfer characteristics of both models influence dielectric properties which in turn impact electromagnetic wave propagation. Although both models in this study are developed under identical assumptions regarding electromagnetic wave propagation, the electrical conductivity and relative permittivity of healthy liver tissue and tumor tissue are temperature dependent. Consequently, variations in SAR distribution are observed between the models.

4.3. Heat transfer analysis

This section presents the heat transfer phenomena within the deformed liver cancer models, comparing the porous media approach with the Pennes bioheat approach. Temperature distribution, a key outcome of heat transfer analysis, is critical to the effectiveness of MWA treatment. This study characterizes heat transfer in the deformed liver cancer models through temperature distribution, which quantifies thermal energy transfer within a specific region. For all examined cases, the treatment duration was set to 10 min, emphasizing heat transfer as a fundamental factor in achieving optimal treatment outcomes.

Fig. 5(a) and (b) present the temperature profiles in the deformed liver cancer models at a treatment duration of 10 min. Fig. 5(a) illustrates the model using the Pennes bioheat approach, while Fig. 5(b) depicts the model using the porous media approach. In both models, the hot spot zone, located around the slot, gradually decreases in intensity with increasing distance from the slot, mirroring the SAR distribution. However, clear distinctions emerge between the two models. The hot spot zone is larger in the Pennes bioheat model, and it also reaches a higher maximum temperature compared to the porous media model, as demonstrated in the figures. Additionally, when tissue deformation is considered, the Pennes bioheat model exhibits greater expansion than the porous media model, even when applying the same scale factor. These differences highlight significant variations in heat transfer phenomena between the two approaches, demonstrating their impact on treatment effectiveness over 10 min of heating.

This section also examines the isothermal contour of 60 °C in both models at 1 min, 3 min, 5 min, and 10 min. Error! Reference source not found.(c) represents the Pennes bioheat model, while Error! Reference source not found.(d) illustrates the porous media model. The 60 °C isothermal contour is selected as a threshold for tissue necrosis onset. The results indicate that the hot spot zone is concentrated around the slot area, with the extent of the isothermal contour and consequently tissue damage expanding with treatment time. However, the two models display notable differences in the extent of the isothermal contour. Specifically, the Pennes bioheat model exhibits a larger hot spot area compared to the porous media model, with this discrepancy becoming

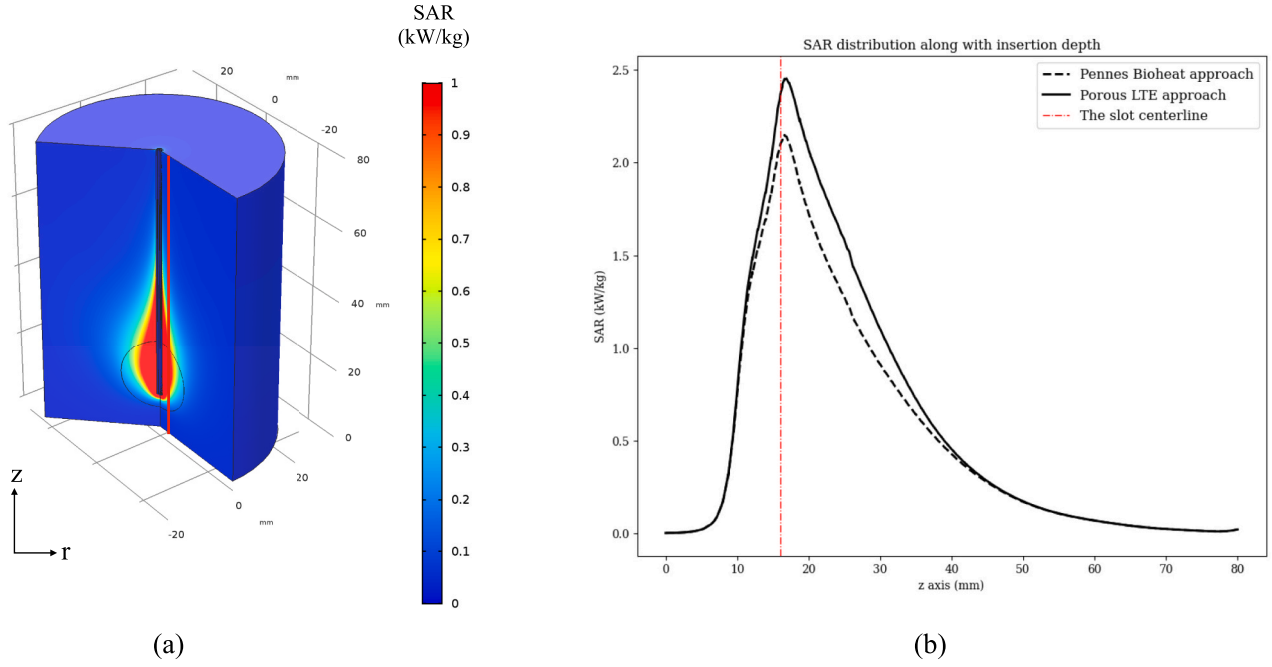

Fig. 4. SAR distribution in the deformed liver cancer model during MWA treatment at 10 min; (a) The SAR profile of the model under the porous media approach, (b) The comparison of SAR distribution of both models along the insertion depth line at the treatment time of 10 min.

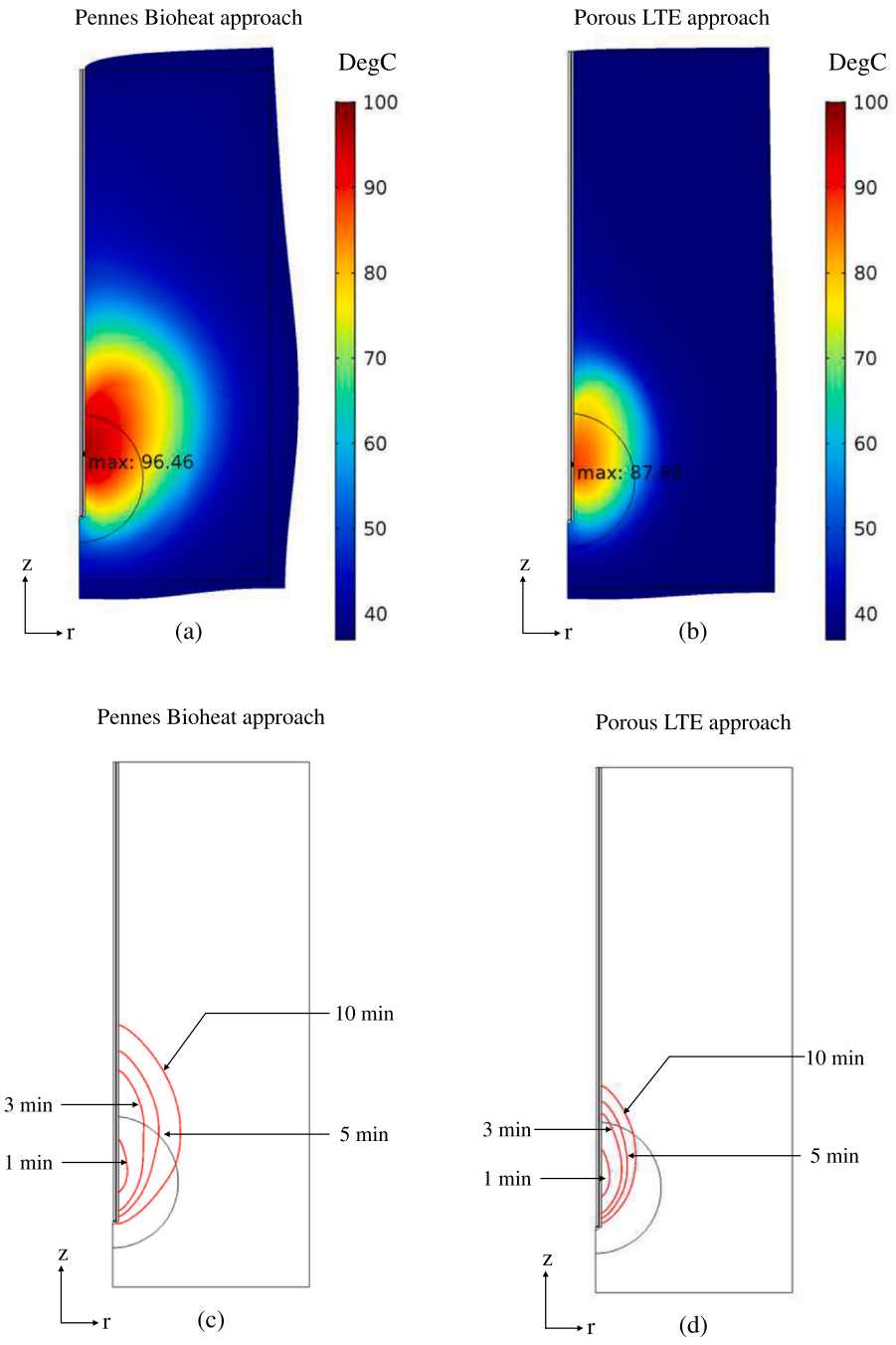

Fig. 5. Temperature distribution in the deformed liver cancer model during MWA treatment; (a) Temperature profile and maximum temperature of the model under the Pennes bioheat approach at a treatment time of 10 min, (b) Temperature profile and maximum temperature of the model under the porous media approach at a treatment time of 10 min, (c) Isothermal contour line of 60 °C for the model under the Pennes bioheat approach, (d) Isothermal contour line of 60 °C for the model under the porous media approach, (e) Temperature distribution of both models along the insertion depth line at treatment times of 1 and 10 min, (f) Temperature distribution of both models along the slot centerline at treatment times of 1 and 10 min.

more pronounced as treatment time increases. This observation suggests that the heat transfer behavior of the two models diverges more significantly over time.

Error! Reference source not found.(e) presents the temperature distribution along the insertion depth line, as previously referenced in Fig. 3(a). This result facilitates a comparative analysis of both models at 1 min, 5 min, and 10 min, revealing that temperature distribution increases with heating time, with a hot spot emerging around the slot center, consistent with the SAR distribution. The mean temperature differences between the two models at 1 min, 5 min, and 10 min are 1.0601 °C, 5.5744 °C, and 8.2195 °C, corresponding to 2.29 %, 9.70 %, and 13.03 %, respectively.

Similarly, Error! Reference source not found.(f) illustrates the temperature distribution along the slot centerline, comparing the two models at 1 min and 10 min. The results indicate that temperature distribution rises with increased heating time, with a hot spot forming

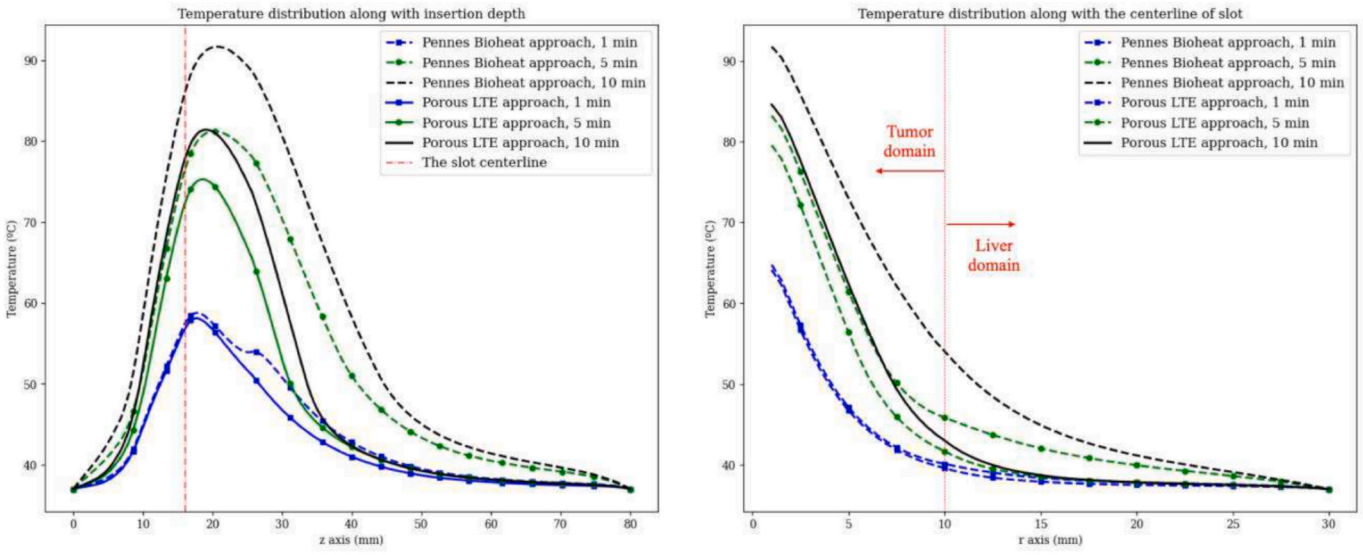

(e) (f)

Fig. 5. (*continued*).

around the slot area. The mean temperature differences between the two models at 1 min, 5 min, and 10 min are 0.3692 °C, 2.9022 °C, and 6.0396 °C, corresponding to 0.88 %, 5.99 %, and 10.91 %, respectively.

The temperature distributions in Error! Reference source not found. (e) and (f) clearly demonstrate that the discrepancy in temperature distribution between the two models becomes more pronounced as treatment time increases. The difference starts at approximately 1 % to 2 % during the initial heating phase and expands to approximately 10 % to 13 % by the end of the 10 min treatment period, depending on microwave power and treatment duration. This finding underscores the dynamic nature of heat transfer during the MWA process.

Furthermore, these results provide insights into the underlying mechanisms of MWA. At the early stage of treatment, heat transfer predominantly occurs through conduction, resulting in similar temperature distributions across both models. However, as treatment time progresses, the heat transfer mechanism in the porous media model transitions from conduction dominated to a combination of convection and conduction. Consequently, the convection term becomes increasingly influential over time, leading to a more pronounced divergence in temperature distribution between the Pennes bioheat model and the porous media model, particularly at longer treatment durations.

4.4. Tissue deformation and tissue damaged analysis

Tissue deformation is a focal point of this study. As tissue temperature increases during the MWA process, thermal expansion leads to tissue deformation. Moreover, previous research has compared MWA models with and without deformation. Their findings highlight a significant difference in temperature predictions between models that incorporate deformation analysis and those that do not. This distinction underscores the critical importance of including tissue deformation in the analysis. This study emphasizes the role of tissue deformation analysis in models utilizing both the Pennes bioheat approach and the porous media approach. Highlighting this comparison is essential in demonstrating the fundamental role of accurate modeling in achieving effective treatment outcomes.

Fig. 6(a) and (b) depict von Mises stress in liver cancer models over 10 min, with Fig. 6(a) representing the Pennes bioheat approach and Fig. 6(b) illustrating the porous media approach. Comparative contours at 1 and 10 min show stress variations over time. The results indicate high stress levels appearing in the tumor tissue near the antenna. A notable difference in stress distribution is observed within the tumor domain between the two models compared to the stress distribution in the healthy liver tissue. Furthermore, stress distribution increases with treatment time, indicating that tissue deformation is closely linked to temperature distribution during treatment. This connection highlights the interaction between thermal effects and mechanical stress in MWA therapy.

Fig. 6(c) and (d) show total deformation in liver cancer models under the Pennes bioheat and porous media approaches over 10 min. Comparative contours at 1 and 10 min illustrate temporal changes. The results indicate an increase in total deformation for both models as treatment progresses. Notably, maximum deformation does not occur within the hot spot zone. This is due to the proximity of the hot spot zone to the antenna, where the tissue is restricted from deforming beyond the antenna due to the significantly higher mechanical properties of the antenna compared to the surrounding tissue. However, as tissue temperature rises, expansion occurs, leading to displacement in areas other than those adjacent to the antenna. Consequently, maximum tissue deformation is observed not within the hot spot zone but in adjacent areas, illustrating the spatial dynamics of tissue response to increased temperatures during treatment. This phenomenon highlights the complex relationship between thermal effects and mechanical constraints in determining tissue deformation patterns.

Fig. 6(e) presents the von Mises stress distribution along the insertion depth line, previously introduced in Fig. 4(a). This comparison enables an evaluation of both models at 1 and 10 min of treatment, revealing an increase in von Mises stress with treatment duration, particularly in the tumor region. The von Mises stress in the model employing the Pennes bioheat approach is higher than in the model using the porous media approach, with the difference becoming more pronounced over time. The mean von Mises stress differences between the two models at 1 min and 10 min are 0.238 Pa and 2.8853 Pa, respectively.

Fig. 6(f) displays the von Mises stress distribution along the slot centerline, comparing the two models at treatment durations of 1 min and 10 min. Consistent with previous findings, stress levels increase over time. Stress values in the tumor domain are higher than in the healthy liver tissue, which can be attributed to differences in mechanical

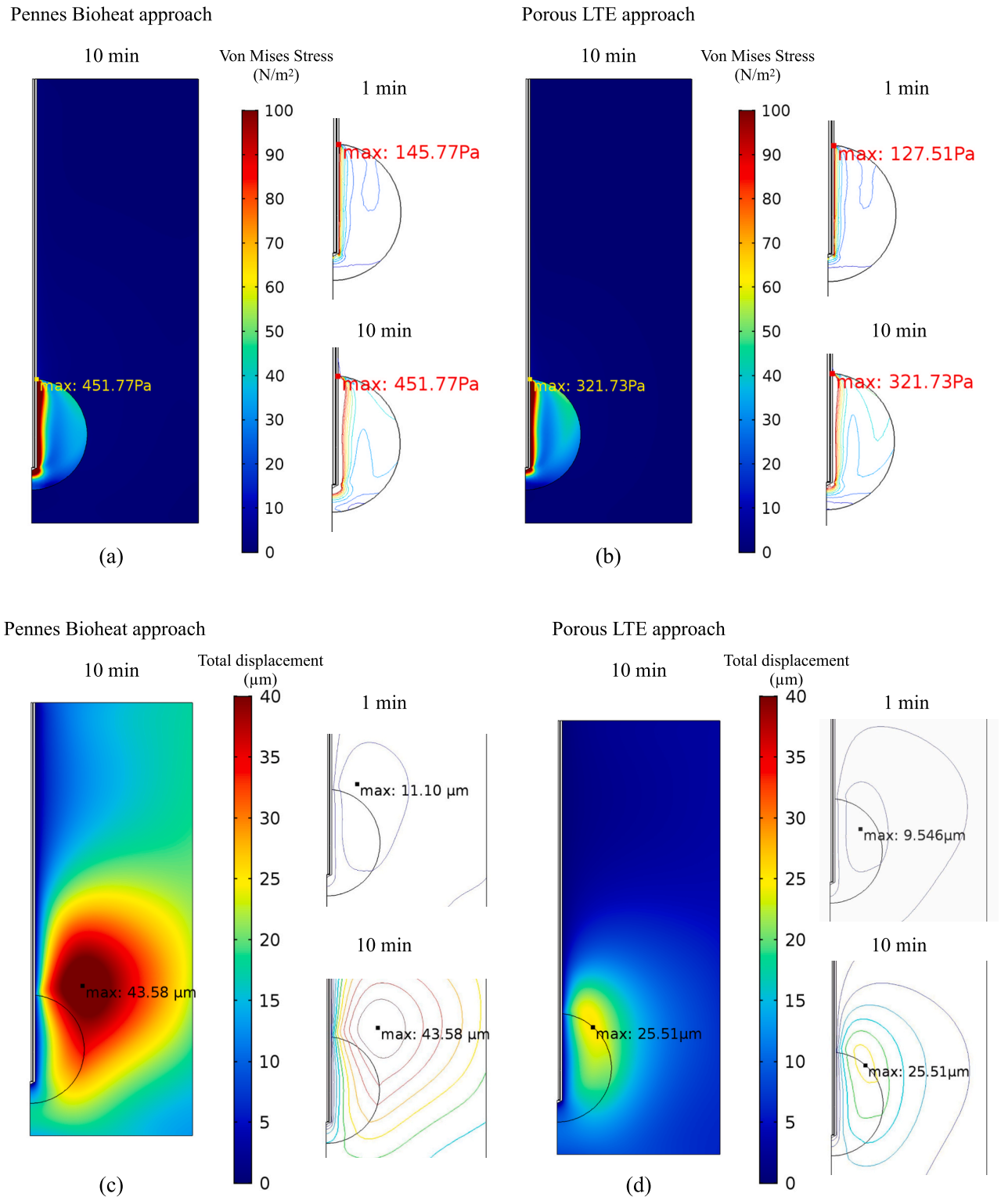

Fig. 6. Von Mises stress and total deformation in the deformed liver cancer model during MWA treatment; (a) Von Mises stress profile and maximum stress of the model under the Pennes bioheat approach, (b) Von Mises stress profile and maximum stress of the model under the porous media approach, (c) Total deformation profile and maximum deformation of the model under the Pennes bioheat approach, (d) Total deformation profile and maximum deformation of the model under the porous media approach, (e) Stress distribution of both models along the insertion depth line at treatment times of 1 and 10 min, (f) Stress distribution of both models along the slot centerline at treatment times of 1 and 10 min.

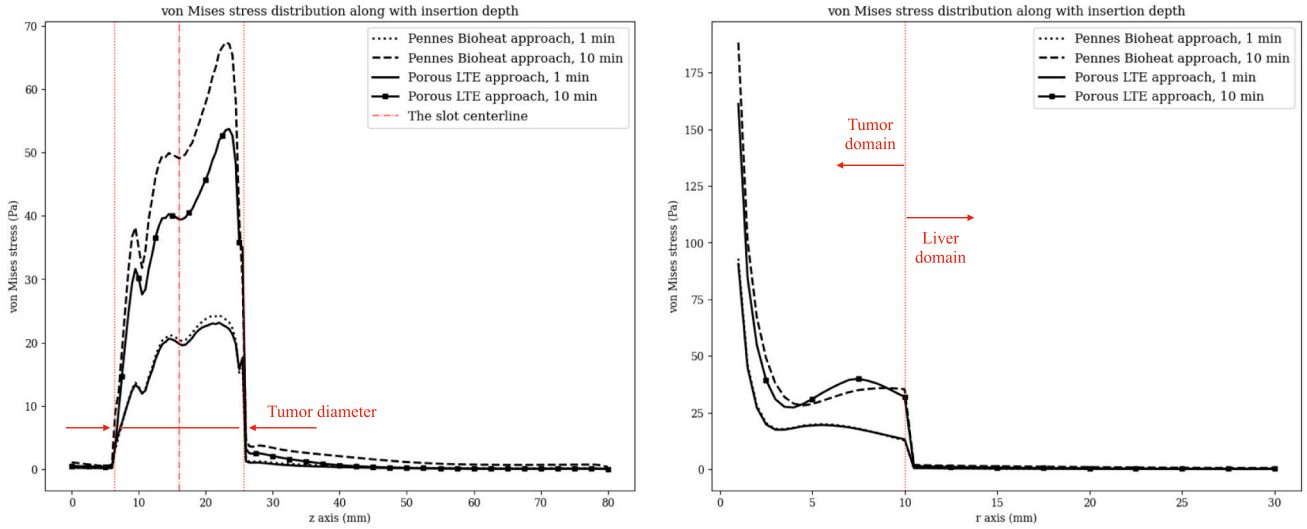

Fig. 6. (*continued*).

properties between tumor and healthy tissue. However, in this direction, the distinction between the models is less pronounced compared to the stress distribution along the insertion depth line shown in Fig. 6(e). The mean von Mises stress differences between the two models at 1 min and 10 min are 0.1668 Pa and 2.2867 Pa, respectively.

Fig. 7(a) illustrates the transient temperatures at points P1 to P4 for both models, with the r z coordinates of these points defined in Fig. 7(c). The points are designated as follows: P1 at coordinates five and twenty represents the tumor area, P2 at 10 and twenty represents healthy liver tissue adjacent to the tumor boundary, P3 at fifteen and twenty represents healthy liver tissue near the tumor, and P4 at twenty and twenty represents healthy liver tissue distant from the tumor. The transient temperatures at points P1 to P4 increase with treatment time, with P1 showing the highest increase, followed by P2, P3, and P4. The temperatures at P1 to P4 in the Pennes bioheat model are higher than those in the porous media model, with the difference increasing over time.

Fig. 7(b) presents the transient von Mises stress at points P1 to P4 for both models, showing significantly higher stress values at P1 compared to the other points. The von Mises stress at P1 ceases to increase after 2 min of treatment, a trend consistent in both models. Additionally, the von Mises stress at P1 in the porous media model is slightly higher than in the Pennes bioheat model. The mean von Mises stress differences between the two models at P1, P2, P3, and P4 are 1.5264 Pa, 0.0637 Pa, 0.2833 Pa, and 0.2879 Pa, respectively.

Fig. 7(c) illustrates the relationship between von Mises stress and temperature increase at points P1 to P4 for both models, highlighting distinct behaviors between the tumor site at P1 and the non-tumor points P2 to P4. At points outside the tumor, an increase in temperature does not necessarily lead to an increase in stress, as seen in P2 in the Pennes bioheat model. In contrast, within the tumor region, stress increases with temperature, as observed at P1 in both models. However, when the temperature increase exceeds approximately fifteen degrees Celsius, the stress at these points no longer rises with temperature, as shown in Fig. 7(c). Additionally, P1 in the porous media model exhibits higher stress values than in the Pennes bioheat model, consistent with findings from Fig. 7(b).

Fig. 7(d) illustrates the extent of thermal damage at points P1 to P4 within both models, revealing significant differences in tissue response. In both models, P1 experiences complete thermal damage over the course of treatment, with the Pennes bioheat model reaching full damage at P1 more quickly than the porous media model. P2 in the Pennes bioheat model also undergoes complete thermal damage but at a slower rate than P1 in either model. In contrast, P2 in the porous media model does not reach complete damage within the treatment duration. This demonstrates the distinct outcomes of thermal damage in liver cancer models treated under the Pennes bioheat and porous media approaches, highlighting the variability in tissue response to MWA therapy.

This study elucidates the differences in tissue deformation and damage in liver cancer models treated under the Pennes bioheat and porous media approaches, as represented by von Mises stress and total deformation metrics. The two models exhibit distinct responses, with variations occurring not only between the approaches but also across different regions within the same model. Initially, stress levels correlate with temperature changes, but this relationship becomes more complex over time, underscoring the intricate interplay between thermal effects and tissue stress. This complexity highlights the critical role of selecting an appropriate heat transfer model in treatment planning to minimize unnecessary damage while maximizing treatment efficacy. These findings emphasize the importance of understanding these complex interactions to enhance the precision and effectiveness of MWA therapy.

5. Conclusion

This study conducts a comprehensive comparison of deformed liver cancer models during MWA, contrasting the Pennes bioheat approach with the porous media approach. The mathematical model integrates electromagnetic wave propagation, heat transfer in biological tissue, tissue damage, and tissue deformation analyses. It encompasses three domains: MCA, the tumor, and the healthy liver tissue. Utilizing a single slot MCA, the model operates at a power of 10 W and a frequency of 2.45 GHz, with a uniform treatment duration of 10 min across all cases. The numerical model is solved using FEM through COMSOL Multiphysics and is validated against experimental results obtained by Yang et al. and through a mesh independence test. To facilitate a clear comparison between models under the Pennes bioheat and porous media approaches, this study investigates the SAR distribution, temperature

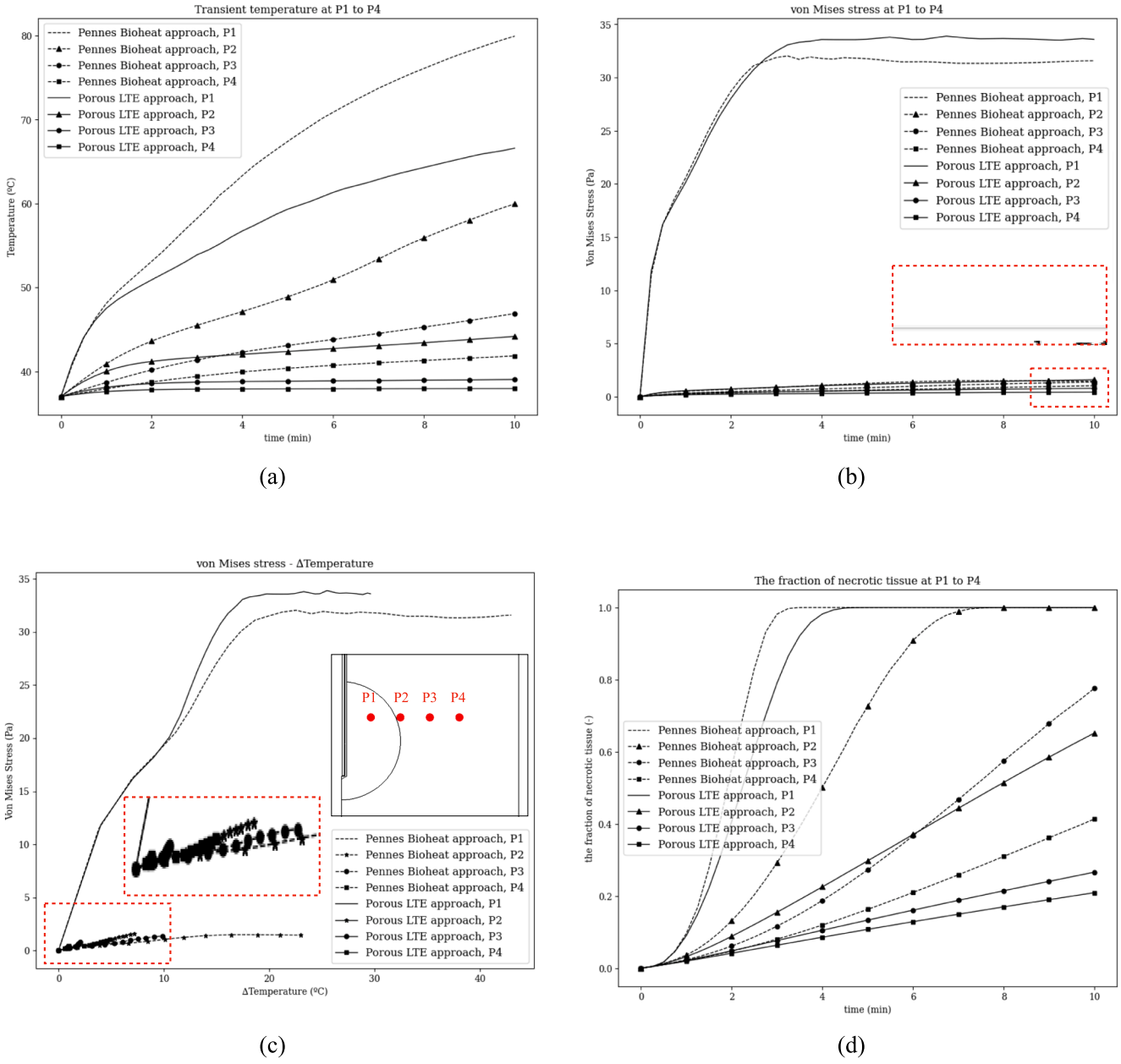

Fig. 7. Transient data of the selected points in the deformed liver cancer models during MWA treatment; (a) The transient temperature, (b) The transient stress, (c) The relation of stress to temperature increase in the deformed liver cancer models, (d) The transient fraction of necrotic tissue during treatment.

distribution, stress distribution, and tissue damage distribution. The key findings are as follows:

1. Both the Pennes and porous media models assume identical initial electromagnetic conditions, yet temperature induced changes in relative permittivity and electrical conductivity lead to local differences in SAR distribution. The porous media model exhibits slightly higher SAR values, particularly near the antenna slot, leading to local variations of approximately 0.0785 kW/kg or 6.72 % across the entire domain. Despite these differences, both models produce a similar water droplet shaped SAR profile, with values peaking around the antenna slot and gradually decreasing outward.
2. Temperature differences between the two approaches remain minimal in the early phase of treatment, staying under 2 % within the first one to two minutes. However, as treatment progresses, the influence of convective effects in the porous media model becomes more pronounced, causing the temperature gap between the two models to widen to approximately 10 % to 13 % by the 10 min mark. The Pennes bioheat model consistently exhibits higher temperatures, particularly in the hot spot region.

3. Peak von Mises stress values appear in the tumor region near the antenna and increase with treatment duration. Stress differences between the models start at approximately 0.2 to 0.3 Pa in the early stages and rise to over 2 Pa in the tumor domain by 10 min. Maximum tissue deformation occurs in areas adjacent to the antenna rather than directly within the hot spot region, due to the mechanical constraints imposed by the antenna.
4. Tumor tissue, particularly at point P1, undergoes complete necrosis in both models, though the Pennes bioheat model reaches this threshold sooner. In contrast, in healthy tissue adjacent to the tumor at point P2, the Pennes model also exhibits complete necrosis, while the porous media model does not reach full necrosis within the same 10 min period. Across all evaluated points, the necrosis progression is consistently faster in the Pennes model compared to the porous media model.

These results demonstrate that the fundamental mechanism of MWA treatment lies in swiftly generating localized heat using electromagnetic wave energy. Initially, both models behave similarly due to the dominance of heat conduction. However, as treatment time extends, the porous media model incorporates enhanced heat convection, which, in combination with conduction, leads to significant differences in heat transport and tissue deformation. This study confirms that tissue deformation analysis significantly influences heat transfer, particularly in the deformed liver cancer model using the porous media approach. The porous media model demonstrates superior representation of heat transport and tissue deformation over medium and longer durations. However, for short duration treatments, the Pennes bioheat model remains a practical choice due to its simplicity and minimal differences from the porous media model, facilitating easier implementation.

In future work, we aim to explore additional factors within the porous media approach that may influence tissue deformation, including porosity, permeability, and the implementation of the local thermal non equilibrium approach. It is hoped that this study provides insight into the distinct phenomena observed in deformed liver cancer models treated with MWA, particularly highlighting the differences in tissue deformation between models utilizing the Pennes bioheat approach and the porous media approach. Understanding these complex interactions will contribute to optimizing MWA treatment strategies for improved clinical outcomes.

CRediT authorship contribution statement

Wutipong Preechaphonkul: Writing – original draft, Visualization, Software, Project administration, Methodology, Formal analysis, Conceptualization. **Vannakorn Mongkol:** Writing – original draft, Visualization, Software, Formal analysis, Data curation. **Arnon Sakonkanapong:** Writing – review & editing, Validation, Supervision, Resources, Investigation, Funding acquisition, Data curation. **Phadungsak Rattanadecho:** Writing – review & editing, Supervision, Resources, Funding acquisition.

Declaration of competing interest

The authors declare the following financial interests/personal relationships which may be considered as potential competing interests: This study was supported by the King Mongkut's Institute of Technology Ladkrabang (KREF046501), KOSEN-KMITL, and the Thailand Science Research and Innovation Fundamental Fund for the fiscal year 2024 and National Research Council of Thailand (Grant Number N42A650197).

Acknowledgement

This study was supported by the King Mongkut's Institute of Technology Ladkrabang (KREF046501), KOSEN-KMITL, and the Thailand Science Research and Innovation Fundamental Fund for the fiscal year 2024, Thailand Science Research and Innovation Fundamental Fund for the fiscal year 2025, and National Research Council of Thailand (Grant Number N42A650197)

Data availability

Data will be made available on request.

References

[1] P. Keangin, P. Rattanadecho, Analysis of heat transport on local thermal non-equilibrium in porous liver during microwave ablation, Int. J. Heat Mass Transf. 67 (2013) 46–60.
[2] M. Selmi, Improved modeling of temperature evolution during lung cancer tumor thermal ablation, Physics 6 (1) (2024) 164–176.
[3] A. Andreozzi, L. Brunese, M. Iasiello, C. Tucci, G.P. Vanoli, Variable porosity-based bioheat model vs variable perfusion-based pennes' equation: a comparison with in vivo experimental data, Therm. Sci. Eng. Prog. 35 (2022) 101469.
[4] X. Wu, B. Liu, B. Xu, Theoretical evaluation of high frequency microwave ablation applied in cancer therapy, Appl. Therm. Eng. 107 (2016) 501–507.
[5] W. Preechaphonkul, P. Rattanadecho, The comparative of the performance for predicted thermal models during microwave ablation process using a slot antenna, Case Stud. Therm. Eng. 25 (2021) 100908.
[6] C. Tucci, M. Trujillo, E. Berjano, M. Iasiello, A. Andreozzi, G.P. Vanoli, Mathematical modeling of microwave liver ablation with a variable-porosity medium approach, Comput. Methods Programs Biomed. 214 (2022) 106569.
[7] H.H. Pennes, Analysis of tissue and arterial blood temperatures in the resting human forearm, J. Appl. Physiol. 1 (2) (1948) 93–122.
[8] X. Li, Q.-H. Qin, X. Tian, Thermo-viscoelastic analysis of biological tissue during hyperthermia treatment, App. Math. Model. 79 (2020) 881–895.
[9] I. Abbas, A. Hobiny, F. Alzahrani, An analytical solution of the bioheat model in a spherical tissue due to laser irradiation, Indian J Phys 94 (9) (2020) 1329–1334, https://doi.org/10.1007/s12648-019-01581-w.
[10] F.S. Alzahrani, I.A. Abbas, Analytical solutions of thermal damage in living tissues due to laser irradiation, Waves Random Complex Media 31 (6) (2021) 1443–1456, https://doi.org/10.1080/17455030.2019.1676934.
[11] A. Hobiny, I. Abbas, Thermal response of cylindrical tissue induced by laser irradiation with experimental study, HFF 30 (8) (2020) 4013–4023, https://doi.org/10.1108/HFF-10-2019-0777.
[12] D. Yang, M.C. Converse, D.M. Mahvi, J.G. Webster, Expanding the bioheat equation to include tissue internal water evaporation during heating, IEEE Trans. Biomed. Eng. 54 (8) (2007) 1382–1388.
[13] P. Keangin, T. Wessapan, P. Rattanadecho, Analysis of heat transfer in deformed liver cancer modeling treated using a microwave coaxial antenna, Appl. Therm. Eng. 31 (16) (2011) 3243–3254.
[14] A.-R.-A. Khaled, K. Vafai, The role of porous media in modeling flow and heat transfer in biological tissues, Int. J. Heat Mass Transf. 46 (26) (2003) 4989–5003, https://doi.org/10.1016/S0017-9310(03)00301-6.
[15] S. Mahjoob, K. Vafai, Analytical characterization of heat transport through biological media incorporating hyperthermia treatment, Int. J. Heat Mass Transf. 52 (5–6) (2009) 1608–1618.
[16] A. Andreozzi, L. Brunese, M. Iasiello, C. Tucci, G.P. Vanoli, Modeling heat transfer in tumors: a review of thermal therapies, Ann. Biomed. Eng. 47 (2019) 676–693.
[17] P. Rattanadecho, P. Keangin, Numerical study of heat transfer and blood flow in two-layered porous liver tissue during microwave ablation process using single and double slot antenna, Int. J. Heat Mass Transf. 58 (1–2) (2013) 457–470.
[18] M. Trujillo, P. Prakash, P. Faridi, A. Radosevic, S. Curto, F. Burdio, E. Berjano, How large is the periablational zone after radiofrequency and microwave ablation? computer-based comparative study of two currently used clinical devices, Int. J. Hyperth. 37 (1) (2020) 1131–1138.
[19] X. Li, Y. Zhong, R. Jazar, A. Subic, Thermal-mechanical deformation modelling of soft tissues for thermal ablation, Biomed. Mater. Eng. 24 (6) (2014) 2299–2310.
[20] V. Mongkol, W. Preechaphonkul, P. Rattanadecho, Photo-thermo-mechanical model for laser hair removal simulation using multiphysics coupling of light transport, heat transfer, and mechanical deformation (case study), Case Stud. Therm. Eng. 41 (2023) 102562, https://doi.org/10.1016/j.csite.2022.102562.
[21] V. Lopresto, R. Pinto, L. Farina, M. Cavagnaro, Microwave thermal ablation: effects of tissue properties variations on predictive models for treatment planning, Med. Eng. Phys. 46 (2017) 63–70.
[22] W. Preechaphonkul, P. Rattanadecho, The effects of dielectric & thermal property functions on the thermal response during the focused microwave ablation treatment in the liver cancer model: numerical investigation, Engineered Science 21 (2) (2022) 788.
[23] P. Yuan, Numerical analysis of temperature and thermal dose response of biological tissues to thermal non-equilibrium during hyperthermia therapy, Med. Eng. Phys. 30 (2) (2008) 135–143.
[24] F. Ti, X. Chen, H. Yang, S. Liu, T.J. Lu, A theory of mechanobiological sensation: strain amplification/attenuation of coated liquid inclusion with surface tension, Acta Mech. Sin. 37 (2021) 145–155.
[25] W.-C. Yeh, P.-C. Li, Y.-M. Jeng, H.-C. Hsu, P.-L. Kuo, M.-L. Li, P.-M. Yang, P.H. Lee, Elastic modulus measurements of human liver and correlation with pathology, Ultrasound Med. Biol. 28 (4) (2002) 467–474.